Kinetics of Water Vapor Sorption in a Model Freeze-Dried Food

P. M. BLUESTEIN and T. P. LABUZA

Department of Nutrition and Food Science
Massachusetts Institute of Technology, Cambridge, Massachusetts 02139

Sorption kinetics experiments were performed at 37 C with microcrystalline cellulose held between dryness and 51% water activity in the absence of other gases. Effective diffusion coefficients ($>10^{-4}$ cm^2/s) were greater than any previously reported for similar experiments. A model based on heat and mass transfer properties of the sample is proposed. The vapor space permeability calculated by application of this model is related to the structure of the microcrystalline cellulose as determined from water desorption isotherm analysis, mercury intrusion porosimetry, and steady state permeability techniques. Microcrystalline cellulose, like some freeze-dried foods, contains micropores and macropores. During sorption, the macropores are important in determining the balance between internal and environmental control during the first half of sorption. The micropores, which account for less than 1% of the void volume of the porous matrix but approximately 40% of the surface area, control the mass transfer properties of the sample during the latter stages of sorption. Because of the great difference between their mass transfer properties, the macropores approach local equilibrium faster than the micropores; this phenomenon suggests that changes in the effective diffusion coefficient and permeability as sorption proceeds are related to the structure of the sample rather than to the moisture content itself.

Drying of foods is a process of major industrial importance. The physical phenomena that occur during drying and the mechanisms of moisture transport are so varied that sorption experiments have been used to study mass transfer in porous and nonporous food materials. Generally, these investigations have been conducted without concern for the environmental resistances to moisture transport or for the conduction of the heat released during sorption from the sample food through the environment to a heat sink, although heat factors have been shown to affect the rate of moisture sorption considerably (*1, 2*).

Many analyses of sorption have been used to calculate a diffusion coefficient based on an appropriate solution of Fick's second law of diffusion, Equation (1).

$$\frac{\partial M}{\partial t} = \frac{\partial}{\partial x}\left(D \frac{\partial M}{\partial x} \right) \tag{1}$$

Crank (3) has presented various solutions of Equation (1) with a constant diffusion coefficient based on appropriate boundary conditions and sample geometry, and he has outlined methods for determining the functional dependence of the diffusion coefficient on the moisture content. This implies, sometimes incorrectly, that the diffusion coefficient is mechanistically related to the moisture content. King (*4*) has shown that the effective diffusion coefficient (D_{EFF}) is related to various physical properties of the sample (k, ΔH_s, ρ_s, etc.). This relationship occurs because sorption is a heat and mass transfer process. As such, any one rate parameter must be related to those properties important to both heat and mass transfer. The present study was undertaken to determine the importance of both heat and mass transfer in this process with attention given to the influence of structure on sorption kinetics.

MODEL

Our model was based on microcrystalline cellulose. Environmental resistances were considered to be negligible. The mass transfer coefficient b was considered to be a vapor space permeability including the mechanisms of Knudsen, slip and viscous flow, and the modifying factors of porosity and tortuosity. King (*4*) has proposed a similar model based on the diffusion of water vapor in another gas and derived an equation relating the effective diffusion coefficient to the physical properties of the sample. If gases other than water vapor are not present and the mechanism of mass transfer is vapor flow, as was the case in these experiments, then the equations derived by King (*4*) can be transformed into Equations (2) and (3).

$$D_{\text{EFF}} = \frac{M_w}{\rho_s} b \left(\frac{\partial a}{\partial M} \right)_T P^0 \frac{\alpha}{1+\alpha}, \tag{2}$$

$$\alpha = \frac{R\,T^2\,k}{b\,a\,P^0\,\Delta H_s^2} \tag{3}$$

Our model was based on the following assumptions: 1. Mass transfer within the sample may be represented by $N = -b\dfrac{\partial p}{\partial x}$. 2. The rate-controlling transport processes are internal heat and mass transfer. 3. The sample is in local equilibrium with the water vapor partial pressure gradient. 4. Surface diffusion is not an important mass transfer mechanism. 5. Sensible heat changes are small compared to the total heat released on sorption. This implies that the temperature change is small and that the physical properties sensitive to temperature (b, k) are

Correspondence concerning this paper should be addressed to P. M. Bluestein at the Laboratory for Physical Technology, Eindhoven Technical University, Netherlands. T. P. Labuza is with the Department of Food Science and Industries, University of Minnesota, St. Paul, Minnesota.

constant in relation to temperature. 6. Certain physical properties of the sample which are known to vary with the moisture content, such as the heat of sorption (5), thermal conductivity (6), and the slope of the isotherm (7), are considered constant over the small range of moisture content used for each calculation. 7. Swelling does not occur as sorption proceeds.

Several other models have been proposed which do not represent the physical situation well. Models based only on a diffusion coefficient do not account for the rather large amount of heat released during sorption (7 to 9). Elovitch kinetics do not approach equilibrium (*10, 11*). Each of these methods for analyzing sorption kinetics may fit the data and allow comparisons between samples, but the mass transfer properties of a porous material can be analyzed, studied, and compared only when external resistances and the effects of the heat released during sorption are eliminated.

PROCEDURE

Materials Used

Microcrystalline cellulose (Avicel, pH 101, FMC Corp.), which is used industrially as a food ingredient, served as a model freeze-dried food system. This material was used because, unlike most freeze-dried foods, it does not absorb moisture and swell, and its structure is stable in a humid environment (as indicated by constant sorption after repeated cycling between dryness and $a = 0.51$).

Kinetics of Sorption

The modified McBain balance used to determine the kinetics of sorption is shown in Figure 1. The all glass equipment was housed in a constant temperature room at 37 ± 0.5 C. The sample of approximately 5 to 8 g was placed in a cylindrical sample pan of aluminum foil and suspended from a calibrated quartz spring (spring constant = 0.030325 g/mm) in the sorption chamber. The equipment was evacuated to below 0.020 torr as measured by thermocouple gauges. After dissolved air was removed from the flasks containing water and saturated salt solution (magnesium nitrate at 37 C, $a = 0.51$, and 24.00 torr), water vapor from the flask containing pure water was admitted into the vapor reservoir to a pressure of 30.00 torr. It had previously been observed that when this pressure in the vapor reservoir was expanded into the sorption chamber, the final pressure was 24.00 torr. Pressures in this range were measured with the manometer filled with a diffusion pump oil (Apiezon B oil, at 37 C, $\rho = 0.864$ g/cc). The length of the spring was then determined to calculate the dry weight. On the admission of water vapor to the sorption chamber, all stopcocks were turned to bring the sample into contact with the vapor from the saturated magnesium nitrate solution. The length of the spring was monitored as the sample approached equilibrium; usually 24 hr were allowed for equilibration. The spring length was used to calculate the weight of the sample corrected for buoyancy and the moisture content as sorption proceeded. Adsorption kinetics (increasing moisture content) were determined, but desorption kinetics could not be obtained because of the entrainment of the powder in the flowing water vapor during desorption.

Steady State Permeability

The steady state permeability of microcrystalline cellulose was determined at 37 C with the equipment in Figure 2. The sample was supported by coarse grade filter paper. Saturated salt solutions (lithium chloride, magnesium chloride, and magnesium nitrate) supplied water vapor at pressures controlled by the manostat to be slightly below the partial pressure of each solution. By this method large water vapor fluxes with their resultant thermal gradients and large pressure drops through the powdered sample were avoided (in practice $\Delta p <$ 1.0 torr). The equipment was evacuated through trap 1 until the pressure reached the desired value and steady state was established. During the period used to determine the steady state flux, water vapor was condensed in traps 2 and 3 which were previously weighed when dry. After each experiment, the traps were defrosted and weighed to determine the flux of water vapor. After the three experiments, the sample was examined; no channels, which would have been caused by excessive pressure drops, were observed. The resistance of the equipment to flow was measured with the equipment assembled as in Figure 2 without a sample and found to be 4.41×10^{-2} s torr/g, which is less than 20% of the resistance of the sample. The permeability of the sample was calculated by

$$b = \frac{L}{M_w A \dfrac{\Delta p}{\Delta w/\Delta t} - R_e} \qquad (4)$$

Physical Properties

Water sorption isotherms in the adsorbing and desorbing directions were determined at 37 C with the modified McBain balance shown in Figure 1. The weight of the sample after evacuation for 24 hr at 37 C was taken as the dry weight. Water vapor was admitted to the sorption chamber and after equilibrium, the length of the spring and the water vapor partial pressure were determined. To determine an isotherm in the adsorbing (increasing moisture content) direction, additional water vapor was admitted after each equilibration. For an isotherm in the desorbing direction, water vapor was removed from the sample by the vacuum pump.

Sorption isotherms in the adsorbing direction were also obtained at 45.3 C, 38.5 C, and 31.5 C by the standard gravimetric procedure and were used to determine the heat of sorption by the method proposed by Othmer and Sawyer (*12*). Samples were equilibrated for at least 48 hr in partial vacuum in desiccators containing various saturated salt solutions. They were then weighed with an analytical balance (Mettler) to the nearest 0.01 mg. The moisture content of the original sample material was calculated by determining the weight lost during

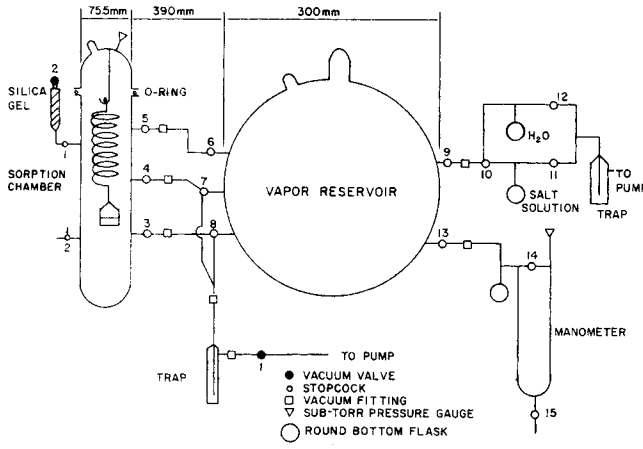

Fig. 1. Modified McBain balance.

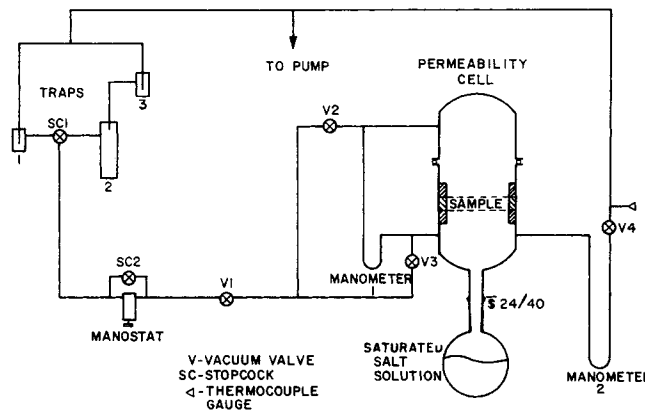

Fig. 2. Steady state permeability apparatus.

drying at 60 C in a vacuum oven at 30 in Hg vacuum. Because of the uncertainty in the isotherm at low moisture content, the heat of sorption was not calculated at moisture contents below 0.02 g water/g solids.

The bulk density and solids density were used to calculate the porosity of microcrystalline cellulose samples. Bulk density was determined by weighing a known volume of powder (± 0.01 g) contained in a graduated cylinder (± 0.25 cc). An air comparison pycnometer (Beckman Model 912A) was used at a pressure of two atmospheres to determine the solids volume.

The thermal conductivity of microcrystalline cellulose was determined at one atmosphere pressure and at an average temperature of 37 C. The equipment resembled that of Wang and Knudsen (*13*). The thermal conductivity found for the sample (2.7×10^{-4} cal/cm s °K) was similar to the thermal conductivity of freeze-dried turkey (*14*).

The structures of the cellulose sample were determined by three methods. Mercury intrusion porosimetry performed on a Carloerba instrument by Numec, Inc. showed anomalous results below a pore radius of 500 Å. Below this radius, the volume intruded decreased as the pressure increased. However, mercury intrusion porosimetry did confirm the presence of approximately 0.3 cc/g of pores with an average pore radius of 0.5 μ. For smaller pores, a desorption isotherm analysis based on the *t*-curves for water vapor sorption available in the literature (*15*) was used. The *t*-curve represents the amount of moisture adsorbed on a similar but nonporous substrate. The difference between the desorption isotherm and the *t*-curve multiplied by the BET monolayer (M_{BET} = 0.0324 g water/g solids) was taken to be the cumulative volumetric pore size distribution. The pore radius just emptying at a given water activity was determined from the Kelvin equation assuming a cylindrically shaped pore:

$$a = e^{-\left[\frac{2\gamma v \cos\theta}{rRT}\right]} \tag{5}$$

The steady state permeability of microcrystalline cellulose was measured over a range of pressures (Figure 3). The relationship, which is linear over the pressure range, was assumed to reflect the flow mechanisms of Knudsen and viscous flow. The intercept and slope of Figure 3 can be used to calculate two average pore radii according to the flow model of Otani et al. (*16*):

$$r = \sqrt{8\epsilon^2 \mu R T \frac{\Delta b}{\Delta p}} \tag{6}$$

$$r = \frac{RT\lambda}{\epsilon^2 2 D_w} \text{ [intercept]} \tag{7}$$

A tortuosity value was not included in these calculations because of the lack of an independent method for its evaluation; the authors believe that the value of tortuosity is a function of the mechanism of flow which is predominating.

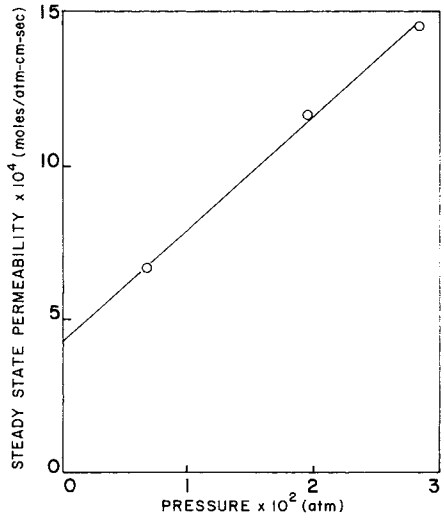

Fig. 3. Steady state permeability of unfractionated microcrystalline cellulose.

Calculations

The calculation of an effective diffusion coefficient for the kinetics of sorption of water vapor by cellulose allowed us to compare the overall sorption rate with the extensive literature on sorption in polymers and foods. The solution to Equation (1) for an infinite plane with the boundary conditions

$$c = c_0' \quad 0 \leq x \leq L, \quad t \leq 0 \tag{8}$$

$$c = c_\infty \quad x = L, \quad t \geq 0 \tag{9}$$

is

$$\Gamma \equiv \frac{M_\infty - M}{M_\infty - M_0} = \frac{8}{\pi^2} \sum_{n=0}^{\infty} \frac{e^{-\left[\frac{-D_{EFF}(2n+1)^2 \pi^2 t}{4L^2}\right]}}{(2n+1)^2} \tag{10}$$

The unaccomplished moisture change Γ was determined from the data of spring length versus time. An iterative procedure on the computer was devised with a maximum error in the effective diffusion coefficient of less than 10^{-7} cm²/s. Effective diffusion coefficients, calculated from each data point, represent the integral of the instantaneous (called specific) effective diffusion coefficient over time since time = zero. Two average values of D_{EFF}, which can be represented as the integral of the specific diffusion coefficient between certain limits of Γ, were found to be useful. The use of a Γ-averaged D_{EFF} is justified on the basis that: 1. there is no real mechanistic relationship between the moisture content and the diffusion coefficient; 2. the use of Γ allows the comparison of runs with different equilibrium moisture contents, representing a normalized driving force; and 3. the model of sorption based on the structure of microcrystalline cellulose suggests that the diffusion coefficient is mechanistically related to the extent of sorption ($1 - \Gamma$) as controlled by the physical properties of the material. The two most useful average effective diffusion coefficients were the integral of D' over the first half of sorption ($0.5 \leq \Gamma \leq 1.0$) D_{half}, and the final stages of sorption ($0.01 \leq \Gamma \leq 0.5$) $\overline{D_f}$.

Analysis of the specific diffusion coefficient D' which represents the overall rate of sorption during a small interval of sorption is complicated by the interactions of heat and mass transfer during sorption. The vapor space permeability b, however, represents only the mass transfer properties of the sample during sorption. Thus, the specific permeability calculated from a rearranged form of Equation (2) was used to represent the mass transfer properties of the sample during sorption. During the small intervals of sorption, the heat of sorption and slope of the isotherm were assumed to be constant and equal to their value at the average value of the moisture content of the interval. Additional information concerning the experimental procedures is available (*17*).

RESULTS AND DISCUSSION

Structure of Microcrystalline Cellulose

The results of isotherm analysis and mercury intrusion porosimetry used to characterize the intraparticle pore size distribution appear in Figure 4. The void volumes measured by isotherm analysis (0.0184 cc/g) and by mercury intrusion porosimetry (0.3 cc/g) were considerably smaller than the total void volume of the packed cellulose (1.99 cc/g). The distribution of pore radii appears to be discontinuous (Figure 4); however, no suitable measurement technique for the radius range between 55 Å and 500 Å was available. Isotherm analysis confirmed the presence of the micropores referred to by Battista (*18*). These micropores are the voids and cracks between microcrystals which are packed in a regular array in each particle (*19*).

The steady state permeability of a cellulose sample as a function of pressure (Figure 3) was used to characterize

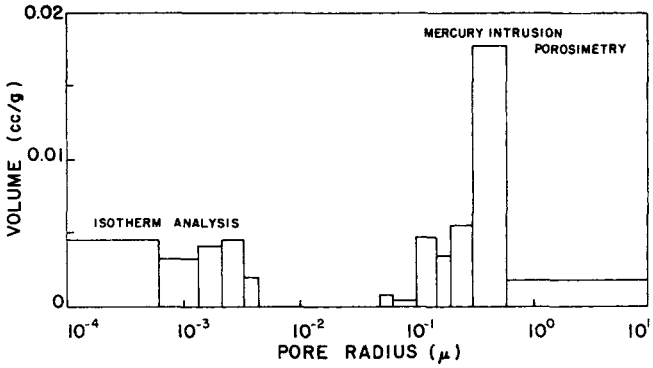

Fig. 4. Intraparticle pore radii distribution.

the macropores. The permeability data are similar to those obtained by Gunn (*20*) for freeze-dried turkey. The mean free path (λ) was estimated from the correlation of Thijssen and Rulkens (*21*). The self-diffusion coefficient of water vapor (D_w) and the viscosity (u) were estimated from the 6-12 potential theory of gases (*22, 23*). The radii calculated from the slope (20.1 μ) and intercept (3.5 μ) differed considerably [Harper (*24*) also found this difference]. The permeability data confirm the presence of large pores with an average radius on the order of 10 μ. This average pore radius is similar to that found in a turkey sample frozen at an intermediate rate (*25*).

The pores confirmed by flow measurements cannot be thought of as interparticle pores only because of the influence of the intraparticle pores measured by mercury intrusion porosimetry. Intraparticle pores, with radii between 500 Å and 10 μ, undoubtedly contributed to the flux during steady state flow. For this reason and because the pores large enough to be measured by mercury intrusion porosimetry had flow properties similar to those of interparticle pores, a classification of pores based on pore radius was developed. This classification and some of the properties of each pore group are listed in Table 1.

The void volume and porosity of the micropores were considerably smaller than those of macropores. The micropore size distribution, measured by isotherm analysis, was used to calculate the surface area of the micropores (based on a cylindrical shape). Although this calculation provides only an estimate, it does show that a considerable amount of the total surface available for sorption (38.6%) is located in the micropores. If the distribution of moisture at equilibrium is based on surface area, then the flow of moisture during kinetics experiments must occur through two different paths. These two locations of sorbed moisture and their different permeabilities affect the kinetics of sorption considerably. This will be discussed after a general discussion of specific permeability and data on the kinetics of sorption.

Kinetics of Sorption

The kinetics of sorption can be characterized by the average effective diffusion coefficients or the relation of the specific diffusion coefficient to Γ. Figure 5 is typical of the relation of D' to Γ. Initially, the specific diffusion coefficient was large and decreased rapidly when Γ was greater than 0.5. When $\Gamma < 0.5$, the specific diffusion coefficient was relatively constant and then decreased suddenly at extremely small Γ. Because the specific diffusion coefficients are related to the thermal effects as well as the mass transfer properties, it is difficult to relate D' to the structure of the sample.

D_{EFF} was calculated with the factor of L^2; we assumed that external resistances to either mass transfer or transfer of the heat released during sorption were negligible. If this assumption was true, D_{EFF} for the same cellulose samples with different thicknesses should be the same. King (*4*) has shown that if external resistances are controlling the kinetics of sorption, D_{EFF} should be a direct function of L. The relationship of two average effective diffusion coefficients to sample thickness is shown in Figure 6. The half-time diffusion coefficient D_{half} is a function of L, indicating that the external resistances to heat and mass transfer strongly influenced the sorption kinetics during the first half of sorption. Because these experiments were performed in the absence of air and in a partial vacuum, the transfer of the heat released during sorption to the environment was considered to be the rate-limiting factor during the first half of sorption. At very low moisture contents, the heat of sorption is high as shown in Figure 7. The rate of heat released during sorption was calculated from Equation (11) and appears in Figure 8. During the first half of sorption

$$q = A\ \Delta H_s\ N \qquad (11)$$

Table 1. Classification of Micropores and Macropores of Unfractionated Microcrystalline Cellulose

	Micropores, $r \leq 100$Å	Macropores, $r \geq 100$Å	Total
Range of pore radii measured	6.4-55Å	500Å-10μ[a]	
Average radius	16Å	10μ	
Void volume, cc/g	0.0184	1.97[b]	1.99
Porosity	0.007	0.729[b]	0.736
Surface area, cm^2/g	44	70[b]	114[c]
Surface area, %	38.6	61.4	100.0
Permeability of a capillary, g-moles/atm cm s	2-5 $\times$ 10^{-6}[d]	3.0 $\times$ 10^{-3}[e]	

[a] Largest pore size is approximate.
[b] Calculated as the difference between the property of the total and the micropore.
[c] BET surface area.
[d] Taken from sorption kinetics experiments.
[e] From steady state permeability studies.

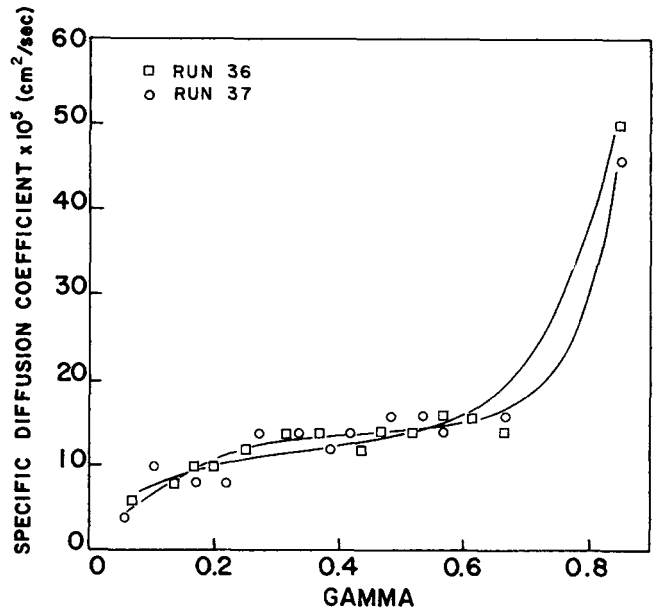

Fig. 5. A typical relationship between the specific diffusion coefficient and gamma (Runs 36 and 37 are duplicate runs).

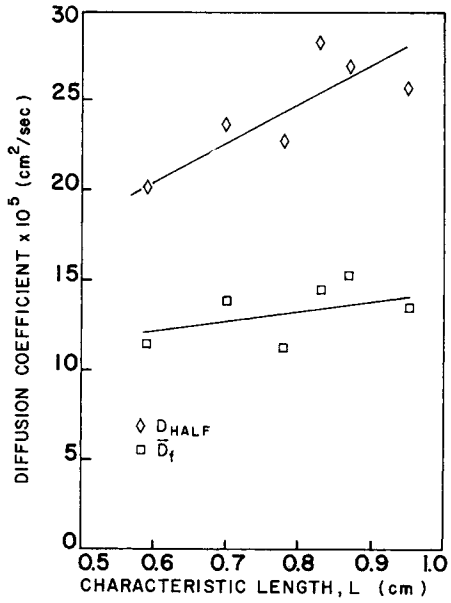

Fig. 6. Average diffusion coefficients of unfractionated microcrystalline cellulose.

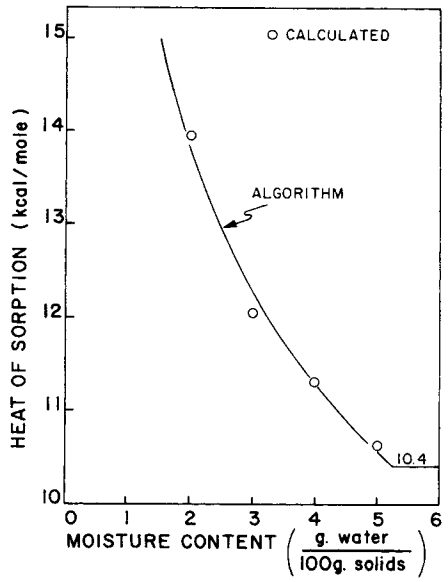

Fig. 7. Heat of sorption of unfractionated cellulose calculated according to (12).

the rate of heat release is approximately 20 times greater than that during the second half of sorption. The heat released either raises the sample temperature or is conducted away through the partial vacuum. Sample temperatures recorded during a sorption experiment showed a transient rise. This elevation occurred for 9 min over a range of Γ from 1.0 to 0.49 and had a maximum ΔT of 3.2 C.

The effective diffusion coefficient characterizing the latter stages of sorption $\overline{D}_f$ is only a slight function of the sample thickness L. The slight slope of the line shown in Figure 6 falls within the expected range, considering the standard deviation of the final diffusion coefficient (1.6×10^{-5} cm²/s). This slight dependence on L indicates that the control of the kinetics of sorption shifts from predominantly external heat transfer to predominantly internal factors. A calculation of the ratio of the internal mass transfer resistance to the internal heat transfer resistance (α) shows that during the latter stages internal mass transfer was the predominantly controlling factor. During the last half of sorption, α varied from 1 to 10. This shift in control results from the decreased rate of heat release and the effect of the micropores as will be shown.

Because of the interactions between heat and mass transfer during sorption, a diffusion coefficient thus cannot be directly related to the structure of the sample. The specific permeability however, calculated from the specific diffusion coefficient, characterizes the mass transfer properties of the sample and shows the same general relationship to Γ as does the specific diffusion coefficient (Figure 9). At earlier stages of sorption, the model proposed is not applicable because of the effects of external resistances to heat transfer. When $\Gamma < 0.5$, specific permeability decreases rapidly as sorption proceeds. During the latter half of sorption, there is a continual gradual decrease in the vapor permeability of the sample. This relationship can be clearly explained by the structure of unfractionated microcrystalline cellulose.

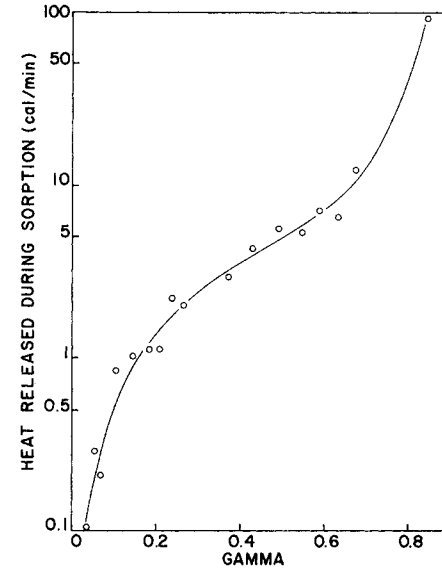

Fig. 8. The rate of heat released during sorption.

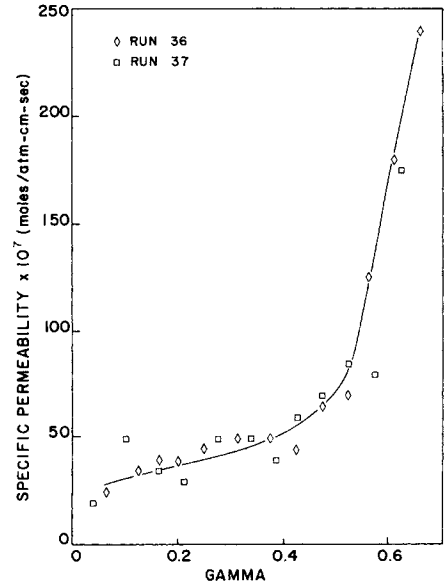

Fig. 9. Mass transfer properties of a microcrystalline cellulose sample during sorption.

The structure of microcrystalline cellulose characterized in Table 1 accounts for the mass transfer properties of cellulose during sorption. The most important factors are the distribution of surface area and the permeabilities of the micropores and macropores. Since at equilibrium under the conditions used (total volumetric adsorption 0.06 cc/g), moisture is distributed throughout the sample on the basis of the surface area distribution, approximately 40% of the moisture is sorbed on the surface of the micropores. The remaining 60% is located on the surface of the macropores. The location of moisture at equilibrium determines both the path of vapor during kinetics experiments and the resistance to mass transfer. Moisture flowing only to the surface of the macropores exhibits a much higher permeability than does moisture which is ultimately sorbed on the micropore surface and therefore must flow through the micropores. Because the permeabilities for flow to sorbing sites in the macropores differ so greatly from the permeability for flow to sites in the micropores, we considered mass transfer during sorption to be two mass transfer processes occurring simultaneously.

Each of the two processes was considered as having the same thermal properties as the total sample but as having two different permeabilities and distributions of moisture. Because all of the cellulose samples had a permeability in the range of 5×10^{-6} g-moles/atm s during the latter stages of sorption, this value alone was used to represent the permeability of flow through the micropores and macropores in series to the surface of the micropores. Specific diffusion coefficients for each sorption process were calculated as a function of Γ by trial and error using these permeabilities and Equations (2) and (3); the coefficients were then used to predict the local Γ in the micropores and macropores. The unaccomplished moisture changes Γ of each location were then added on the weighted basis of the surface area distribution. The surface area distribution was included as a variable because of the uncertainty of the values listed in Table 1. The overall unaccomplished moisture change of the sample, constructed for these two sorption processes, was then analyzed and the specific permeability was calculated. The results of this analysis and actual experimental data appear in Figure 10. The analysis of two sorption processes is shifted slightly higher than the actual data because the permeability used to represent the micropores is slightly larger than the final permeability of Run 46. The shape of the curve in Figure 10 for 40% surface area located in the micropores is in excellent agreement with the actual data. During the early stages of sorption, the specific permeability of the 40% surface area curve decreases rapidly. In the analysis, the assumption of a constant permeability for all the micropores has resulted in a constant permeability during the latter stages of sorption. If a distribution of permeabilities (which is closer to reality) had been used in the analysis, the data of Run 46 and the calculated line for 40% surface area would have agreed more closely. Considering the uncertainty of the procedure for estimating the surface area, the analysis and results agree very well.

The changes in permeability as sorption proceeds result from the different locations of sorption and the permeability to flow for sorption at each location. During the first half of sorption, most of the moisture flows to sorbing sites located on the surface of the macropores. The permeability of this flow path is large ($\simeq 10^{-3}$ g-moles/atm cm s) and the amount of heat released is so great that external heat transfer becomes a controlling factor. As sorption proceeds toward equilibrium ($\Gamma \rightarrow 0$), the surface of the macropores

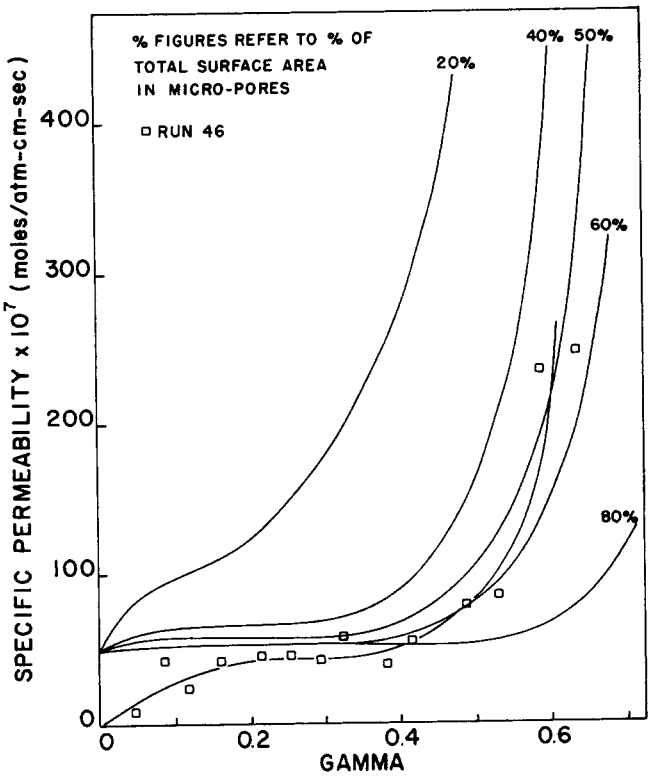

Fig. 10. Two independent simultaneous sorption processes—effect of surface area distribution.

approaches local equilibrium first. Then the micropores begin to influence sorption. The decreased mass transfer permeability of the micropores effects the shift from external heat transfer control of sorption to internal mass transfer control. This shifting of control from predominantly external heat transfer to predominantly internal mass transfer during sorption was seen in the analysis of the diffusivities.

Comparison with Freeze-Dried Foods

The analysis of sorption presented here is quite different from the data available in the literature concerning sorption in dried foods. Diffusion coefficients available for freeze-dried apple and potato are about 2×10^{-6} cm^2/s and characterize the first half of sorption (8). King (4) has suggested that these values were obtained in experiments where external resistances were controlling, so that the mass transfer properties of the foods were not actually being measured. Since most dried foods are likely to have pores with radii on the order of 10 μ (25), the kinetics during the first half of sorption were probably strongly influenced by external resistances like those found for microcrystalline cellulose. The fact that the diffusion coefficients in the literature are 1.5 orders of magnitude lower than those reported here suggests that the equipment used by Saravacos (8) had a greater influence on sorption kinetics than did our equipment.

The analysis of sorption as two independent sorption processes may be applicable, with some modification, to freeze-dried foods. Pycnometric methods have disclosed micropores with a diameter of about 4 Å in a variety of freeze-dried foods (26) and dried milk products (27, 28). However, not all freeze-dried foods have been found to contain micropores of that size (26). In addition, dried foods sorb moisture internally (29), and moisture located inside the solids of the dried food has a greatly reduced diffusion coefficient (30). Therefore, any model of sorption kinetics similar to the one presented here must consider

the location of sorbed moisture at equilibrium. Preliminary results for both adsorption and desorption with commercially available spray- and freeze-dried coffees have shown the typical decrease in the specific diffusion coefficient as sorption proceeds. Unfortunately, methods are not available for the estimation of the relative amounts of moisture sorbed at the three possible locations: on the surface of the macropores, on the surface of the micropores, and inside the food solids. Without these estimates of the relative amounts of moisture sorption, our analysis of sorption kinetics cannot be applied quantitatively.

SUMMARY

Sorption kinetics with microcrystalline cellulose was analyzed as a heat and mass transfer phenomenon. Heat transfer cannot be ignored because it has a large influence during the first half of sorption. During the second half of sorption, control shifted toward internal mass transfer. The effects of the structure of microcrystalline cellulose on sorption were shown. The macropores indirectly effect the rate of sorption during the first half of sorption. The micropores, which account for less than 1% of the void volume but about 40% of the surface area, effect the latter stages of sorption. Application of this analysis to freeze-dried foods may have to be modified to include the additional location of moisture in the solids.

ACKNOWLEDGMENTS

This work was supported in part by a grant from CPC International. P. M. Bluestein wishes to acknowledge the financial support of an NIH Public Health Service Training Grant (FD 000003) and an IFT Fellowship sponsored by the Monsanto Company.

NOTATION

a = water activity, $a = p/P^0$
A = area of the sample, cm^2
b = vapor space permeability, g-moles/atm cm s
c = concentration, g/cc
D = diffusion coefficient, cm^2/s
D_{EFF} = effective diffusion coefficient, cm^2/s
$\overline{D}_f$ = final diffusion coefficient, cm^2/s
D_{half} = diffusion coefficient which characterizes the first half of sorption, cm^2/s
D_w = self-diffusion coefficient of water vapor, cm^2/s
D' = specific diffusion coefficient, cm^2/s
k = thermal conductivity of the sample, cal/cm s °K
L = characteristic length or thickness of the sample, cm
M = moisture content, g water/g solids
M_W = molecular weight of water, 18 g/g mole
N = molar flow rate, g mole/s cm^2
p = partial pressure of water vapor, atm
P^0 = vapor pressure of water, atm
q = heat released during sorption, cal/s
r = capillary or pore radius, cm
R = gas constant
R_e = resistance of the equipment to flow, 4.41×10^{-2} hr torr/g
t = time, s or hr
T = temperature, °K
v = molar volume of water, cc/g-mole
w = weight, g
x = distance, cm

Greek Letters

α = ratio of the internal mass transfer resistance to the internal heat transfer resistance defined by Equation (3)
γ = surface tension of water, dynes/cm
Γ = unaccomplished moisture change, defined by Equation (10)
ΔH_s = heat of sorption, cal/g-mole
ϵ = porosity
θ = contact angle
λ = mean free path, cm
μ = viscosity, g/cm s
ρ_s = bulk density, g/cc

Subscripts

0 = initial quantity
∞ = equilibrium quantity

LITERATURE CITED

1. Armstrong, A. A., Jr., and V. Stannett, *Makromol. Chem.*, **90**, 145 (1966).
2. Armstrong, A. A., Jr., J. D. Wellons, and V. Stannett, *ibid.*, **95**, 78 (1966).
3. Crank, J., "The Mathematics of Diffusion," Clarendon Press, Oxford (1956).
4. King, C. J., *Food Technol.*, **22**, 509 (1968).
5. Makower, B., *Ind. Eng. Chem.*, **37**, 1018 (1945).
6. Saravacos, G. D., and M. N. Pilsworth, *J. Food. Sci.*, **30**, 773 (1965).
7. Saravacos, G. D., and R. M. Stinchfield, *ibid.*, 779.
8. Saravacos, G. D., *ibid.*, **32**, 81 (1967).
9. ———., *Food Technol.*, **16**, 78 (1969).
10. McLintock, I. S., *Nature*, **216**, 1204 (1967).
11. Park, S. W., D. S. Chung, and C. A. Watson, *Cereal Chem.*, **48**, 14 (1971).
12. Othmer, D. F., and F. G. Sawyer, *Ind. Eng. Chem.*, **35**, 1269 (1943).
13. Wang, R. H., and J. G. Knudsen, *ibid.*, **50**, 1667 (1958).
14. Triebes, T. A., and C. J. King, *Ind. Eng. Chem. Process Design Develop.*, **5**, 430 (1966).
15. Hagymassy, J., Jr., S. Brunauer, and R. Sh. Mikhail, *J. Colloid Interfac. Sci.*, **29**, 485 (1969).
16. Otani, S., N. Wakao, and J. M. Smith, *AIChE J.*, **11**, 439 (1966).
17. Bluestein, P. M., Ph.D. thesis, Mass. Inst. Technol., Cambridge (1971).
18. Battista, O. A., *J. Polymer Sci.*, **9**, 135 (1965).
19. Raynor, G. E., Jr., personal communication, FMC Corp., American Viscose Division, Marcus Hook, Pa. (1971).
20. Gunn, R. D., Ph.D. thesis, Univ. California, Berkeley (1967); Gunn, R. D., and C. J. King, *Chem. Eng. Progr. Symp. Ser. No. 108*, **67**, 94 (1971).
21. Thijssen, H. A. C., and W. H. Rulkens, *Ingenieur*, **80**, 45 (1968).
22. Herschfelder, J. O., C. F. Curtiss, and R. B. Bird, "Molecular Theory of Gases," Wiley, New York (1954).
23. Reid, R. C., and T. K. Sherwood, "The Properties of Gases and Liquids," p. 270, McGraw-Hill, New York (1958).
24. Harper, J. C., *AIChE J.*, **3**, 298 (1962).
25. King, C. J., W. K. Lam, and O. C. Sandall, *Food Technol.*, **22**, 1302 (1968).
26. Berlin, E., P. G. Kliman, and M. J. Pallansch, *J. Agr. Food Chem.*, **14**, 15 (1966).
27. Berlin, E., and M. J. Pallansch, *J. Dairy Sci.*, **46**, 780 (1963).
28. Berlin, E., B. A. Anderson, and M. J. Pallansch, *ibid.*, **51**, 668 (1968).
29. Labuza, T. P., *Food Technol.*, **22**, 263 (1968).
30. Margaritus, A., and C. J. King, *Chem. Eng. Prog. Symp. Ser. No. 108*, **67**, 112 (1971).

Manuscript received August 9, 1971; revision received February 23, 1972; paper accepted February 23, 1972.